International Journal of Biological Macromolecules 114 (2018) 1109–1116

Contents lists available at ScienceDirect

International Journal of Biological Macromolecules

journal homepage: http://www.elsevier.com/locate/ijbiomac

Stimulus-responsive zinc oxide-functionalized macromolecular humic acid nanocarrier for enhancement of antibacterial activity of ciprofloxacin hydrochloride

Gowri Murugesan [a], Nachimuthu Latha [a,*], Kannan Suganya [b], Marudhamuthu Murugan [b], Murugan A. Munusamy [c], Mariappan Rajan [d,**]

[a] Department of Chemistry, Kandaswami Kandar's College, Paramathi Velur, Namakkal District, Tamil Nadu 638182, India
[b] Department of Microbial Technology, School of Biological Sciences, Madurai Kamaraj University, Madurai, Tamil Nadu 625021, India
[c] Department of Botany and Microbiology, College of Science, King Saud University, Riyadh 11451, Saudi Arabia
[d] Biomaterials in Medicinal Chemistry Laboratory, Department of Natural Products Chemistry, School of Chemistry, Madurai Kamaraj University, Madurai, Tamil Nadu 625021, India

ARTICLE INFO

Article history:
Received 18 January 2018
Received in revised form 11 February 2018
Accepted 21 March 2018
Available online 22 March 2018

Keywords:
ZnO nanoparticles
Humic acid
Ciprofloxacin

ABSTRACT

Macromolecular of naturally occurring humic acid (HA) have garnered interest in the chemical, biological and medicine industry owing to their unique behavior, *i.e.*, strong adsorptive and non-toxic nature. Here, we investigated the functionalization of organic (HA) with inorganic (ZnO) hybrid nanoparticles for topical and site-targeted delivery of ciprofloxacin by simple emulsification techniques. Ciprofloxacin (CIPRO)-encapsulated hybrid nanocarrier constitute an attractive novel drug delivery vehicle for sustained release of antibiotics to bacterial infection sites in an extended and controlled manner. The analytical characteristics of the designed system were thoroughly investigated by FTIR, XRD, SEM/EDAX, and TEM. The drug release of ciprofloxacin over 24 h was 87.5%, 98.03%, 97.44%, and 97.24% for pH 2.5, 5.5, 6.8, and 8.0, respectively. The antibacterial activities results confirmed that the CIPRO-encapsulated hybrid nanocarrier showed excellent growth inhibition against microorganisms. This hybrid nanocarrier loaded with antibiotics represents a promising approach for targeted and controlled drug delivery to infected sites.

1. Introduction

Treatment with antimicrobial agents, in particular antibiotics, is presently the handiest approach to kill or inhibit the growth of pathogenic microorganisms [1]. However, formulations and derivatization of the effectiveness of existing antibiotics is diminishing because of the fast emergence of new antibiotic agents [2]. The clinical treatment failure of bacterial infections disorder is related to the low bioavailability of cell/tissue-specific barriers, drug stability, biofilm-related infection, and emergence of resistant bacteria [3]. Furthermore, to circumvent the issues of drug resistance, high doses of antibiotics are often administered, generating many side effects and toxicity [4]. Toxicity to healthy tissues and solubility problems are additional limitations of the use of antibiotics in large quantities [5]. In most people, drug absorption occurs at the small intestine because of the large surface area [6]. To conquer drug resistance, antibiotic-encapsulated nanosystems are currently undergoing trials. The activity of antibiotics may additionally be enhanced by pH, enzymatic inactivation, and so forth.

Drug delivery may be performed using various nanostructures, including dendrimers, liposomes, polymers, and hybrid nanoparticles, developed particularly to improve the antimicrobial efficacy of antibiotics by changing their pharmacokinetics and biodistribution profiles [7–9]. Biodegradable materials are non-toxic, biocompatible, and provide a simple manner of controlling the discharge of drugs, using diffusion or swelling [10]. Usually, antimicrobials kill microorganisms by binding to a few of their vital compounds. Humic acid (HA) have attracted huge interest in chemical, biological and medicine industry owing to their unique behavior, including nanoscale, strong adsorption, and non-toxicity [11,12]. HA, produced by the biodegradation of dead organic matter, are ever-present in the natural environment [13]. HA mainly contains —OH and —COOH groups [14]. pH-sensitive HA has greater adsorption capacity because of its high surface area of metal ions. The adsorption of drug molecules on the carrier is carried out *via* susceptible chemical interactions such as hydrogen bonds and Vander Waals forces [15].

* Correspondence to: N. Latha, Department of Chemistry, Kandaswami Kandar's College, Paramathi Velur, Namakkal District, Tamil Nadu 638182, India.
** Correspondence to: M. Rajan, Biomaterials in Medicinal Chemistry Laboratory, Department of Natural Products Chemistry, School of Chemistry, Madurai Kamaraj University, Madurai 625021, India.
E-mail addresses: lathaankl@gmail.com, (N. Latha), rajanm153.chem@mkuniversity.org. (M. Rajan).

https://doi.org/10.1016/j.ijbiomac.2018.03.120
0141-8130/

Ciprofloxacin (CIPRO), a member of the fluoroquinolone family, has broad antimicrobial activity [16]. It is generally used for the treatment of complex and straightforward urinary tract, skin/pore, bone/joint, periodontal, and intestinal infections [17]. At high pHs, CIPRO acquires a negative charge owing to deprotonation of its carboxylic group, whereas at low pHs, CIPRO molecules emerge as positively charged owing to protonation of its amine group [18]. The negatively charged walls of many forms of bacteria intermingle with the positively charged nanostructures *via* electrostatic interactions, affecting permeability adjustments or even the destruction of the entire cell wall and, hence, the pathogen itself [19].

To further increase the performance and properties of antibacterial nanoparticles (NPs), they are gradually combined with other types of metals to form hybrid complexes for sophisticated applications. More recently, inorganic NPs were determined to display strong antimicrobial properties [20]. The property of metal NPs specially depends on their size, stability, and concentration in the medium. Zinc oxide nanoparticles (ZnO NPs) are attractive owing to their low toxicity, low cost, and potential biocompatibility [21]. The biomedical applications of ZnO NPs range from diagnostics to therapeutics. ZnO NPs have unique properties such as semiconducting; wound healing, antifungal, and antibacterial activities [22]. ZnO NPs have well-defined anti-bacterial activities and can be used as an effective bactericidal agent [23]. Single-component materials can only meet few of the multiple desired characteristics. To overcome these challenges, herein, we developed exceptional naturally occurring organic components of functionalized HA with ZnO NPs to encapsulate CIPRO, using a simple emulsion technology. This developed method had been applied in drug delivery systems for controlled, long-term constipation, and targeted drug delivery.

2. Materials and methods

2.1. Materials

Zinc nitrate ($ZnNO_3$), Potassium hydroxide (KOH), Humic acid (HA) (Molwt *ca.* ≈1500), and Sorbitanmonolaurate (Span 20) were purchased from Sigma Aldrich Chemicals, Mumbai, India. Analytical grade chemicals were used without further purification. CIPRO was obtained from Himedia Laboratories (Mumbai, India). Double-distilled water was used throughout the experiments.

2.2. Synthesis of ZnO nanoparticles and functionalization of HA

The preparation of ZnO NPs, functionalization of the nanocarrier, and loading of the antibiotic were carried out by the following steps. Initially, ZnO NPs were prepared by the precipitation method [24] as follows: Briefly, 1.5 M of KOH was prepared by dissolving 8.4165 g of KOH in 100 mL deionized water in a beaker. Then, 14.8745 g of $ZnNO_3$ was dissolved in 100 mL deionized water (0.5 M), transferred to the beaker containing the KOH solution, and magnetically stirred for 1 h (hour). After 1 h, white precipitates of ZnO NPs were obtained, centrifuged at 4000 rpm, and washed thrice with distilled water. Then the precipitates were collected and calcined at 500 °C in a muffle furnace for 4 h. For functionalization, 500 mg of ZnO NPs were dissolved in a beaker containing DMSO, with 1.0 g of HA added, and magnetically stirred for 30 min. ZnO-functionalized HA (hybrid nanocarrier) was collected and centrifuged at 3000 rpm and dried in an air oven at 60 °C for 4 h.

The nanocarrier synthesis and CIPRO encapsulation on hybrid nanocarrier was carried out using the O/W emulsion method [25]. Briefly, 500 mg of ZnO-HA was dissolved in 10 mL of DMSO, and 500 mg of Span 20 was dissolved in 50 mL of water. The DMSO-containing ZnO-HA solution was drop wise added into the water-containing surfactant solution. The mixture was stirred for 2 h and centrifuged, and then dried in an air oven at 60 °C for 4 h, for further characterization. The above procedure was followed by the encapsulation of 250 mg of CIPRO in 500 mg of ZnO-HA nanocarrier, by combining ZnO-HA with the oil portion of DMSO dissolved CIPRO.

2.3. Physico-chemical characterization of hybrid nanocarrier

The functional group of the synthesized compounds was determined using Fourier transform infrared spectroscopy (Spectrum GX-I, Perkin Elmer, Waltham, MA, USA) in the range of 4000–400 cm^{-1}, by the KBr pellet method. Plane orientation and crystalline structure were confirmed by X-ray diffraction techniques (PW3040/60 X pert PRO, Almelo, Netherlands). Surface morphology (Hitachi-SU 6600 Scanning Electron Microscope, Tokyo, Japan; operated at 15 kV) was performed by scanning electron microscopy. The size and shape of the particles were analyzed by transmission electron microscopy operated at 200 kV.

2.4. Estimation of encapsulation efficiency

Nanocarrier and free drug were subjected to the drug encapsulation process. From this reaction mixture, the supernatant solution was collected at 10-min time intervals and centrifuged at 3000 rpm. The concentration of the drug in the solution was analyzed by UV spectrometry (UV-1600, Shimazhu, Japan) with a λ_{max} value of 295 nm. The experiment was performed in triplicate.

$$EE(\%) = \frac{\text{Total amount of drug} - \text{Free amount of drug}}{\text{Weight of dry nanoparticles}} \times 100$$

2.5. Investigation of in-vitro drug release

CIPRO (200 mg)-loaded dry nanocarriers were added to 1 mL of acetate and phosphate buffered saline (pH 2.5, 5.5, 6.8, and 8.0), and then placed inside a dialysis bag, tied at both ends, and dipped in a beaker containing 150 mL of release medium. The beaker was kept in a magnetic stirrer operated at100 rpm. Every 30 min, 3 mL of the *in-vitro* release medium was removed from the beaker and immediately replaced with fresh medium. Release properties of CIPRO were evaluated using UV spectroscopy (UV-1600, Shimazhu, Japan).

2.6. Effect of in-vitro antibacterial activity

2.6.1. Strains and culture conditions

Pseudomonas aeruginosa (*P. aeruginosa*) (ATCC 25619) and *Bacillus cereus* (*B. cereus*) (ATCC 11778) were used as the test bacterial pathogens. Both the pathogens were cultivated and maintained in tryptic soy broth (TSB) containing 0.5% glucose (pH 7 ± 0.2) at 37 °C. Cultures were inoculated from overnight inoculum at a dilution of 1/100 and incubated at 37 °C with shaking at 170 rpm. For all investigates, cultures were grown to mid-exponential phase (optical density at 600 nm [OD600] = 1.2).

2.6.2. MIC and MBC determination

The vulnerabilities of planktonic cells of *P. aeruginosa* and *B. cereus* to the drug and drug-loaded carrier were determined by microtiter broth dilution, as described by the Clinical and Laboratory Standards Institute. Inhibition assays were performed in sterile 96-well plates (Corning Co., NY, USA) in a final volume of 150 μL, comprising 50 μL of microbial cultures (3×10^6 CFU/mL) and 100 μL of the consecutively diluted drug and drug-loaded carrier complexes (1–500 μg/mL). Microtiter plates were statically incubated at 37 °C for 24 h, and the bacterial growth was evaluated by measuring the optical density of the cultures at 600 nm, using a Spectra max microtiter plate reader (molecular devices, Sunnyvale, USA). All inoculums were grown in triplicate. MICs were denoted as the lowermost drug concentration that produced no visible growth after 24 h. Minimum bactericidal concentration (MBC) was calculated by dispersing 100 μL of bacterial cultures from MIC assay microtiter

wells onto Mueller Hinton Agar (MHA) plates and incubating at 37 °C for 12–18 h. The lowest concentration of drug that allowed the formation of less than five colonies on each plate was measured as the MBC. After 24 h of growth, the highest concentration of the drugs and drug-loaded carrier that did not hinder the growth of *P. aeruginosa* and *B. cereus* was selected as the sub-MIC.

2.6.3. Time-kill kinetics against P. aeruginosa and B. cereus

Time-kill kinetics against *P. aeruginosa* and *B. cereus* were recorded for 24 h at concentrations equivalent to the corresponding MIC and 2× MIC for the drug and drug-loaded carrier. *P. aeruginosa* (2.0×10^5 CFU/mL) and *B. cereus* (3.0×10^2 CFU/mL) were incubated at 1× MIC of the drug and drug-loaded carrier at 37 °C and withdrawn at definite time intermissions for viable plate counts. Serial tenfold dilution was made using MH broth. From each dilution, 50 μL was spread superficially onto the MHA plates, and the plates were incubated for 24 h at 37 °C. After incubation, the bacterial colonies were counted and represented as colony forming units per milliliter (Log), to plot a time-growth curve.

2.6.4. Crystal violet biofilm assay and HCS-live biofilm staining with Hoechst

An inert biofilm development assay was performed in 96-well polystyrene plates (Corning Co., NY, USA). Briefly, cells were inoculated into brain heart infusion medium at an initial turbidity of 0.07 (OD600) and cultured with or without the drug and drug-loaded carrier for 48 h without shaking. Biofilms in 96-well plates were gently washed with Milli-Q water and fixed with 200 μL of methanol (99%). Subsequently, the methanol was discarded, and the wells were dehydrated at 28 °C. Crystal violet (0.1%) was then added to each well, and the plates were incubated for 30 min at room temperature. Crystal violet was then removed, and stained biofilms were washed with water. Acetic acid (33%) was added to the stained biofilms to solubilize the crystal violet, and the absorbance of the solution was measured at 590 nm, using a Spectramax microtiter plate reader. The biofilm inhibition percentages were calculated as

$$\%\text{Biofilm inhibition} = \left[1 - \frac{Ac}{Ao}\right] \times 100$$

where Ac represents the absorbance of the well with a particular drug concentration C, and Ao denotes the absorbance of the control well.

2.6.5. Motility and colony-spreading assay

The motility assay was performed by following the method described by Suganya et al. [26]. Five microliters (OD adjusted to 0.4 at 600 nm) of *P. aeruginosa* and *B. cereus* was point-inoculated into the midpoint of the soft agar medium (1% peptone, 0.5% NaCl, 0.5% agar, and 0.5% of filter-sterilized D glucose) with (1/2 MIC) and without the drug and drug-loaded complex. The plates were then incubated at 30 °C in a vertical orientation for 12 h and analyzed for reduction in the areas of colony immigration regions.

3. Results and discussion

3.1. FTIR analysis

The presence of functional groups in antibiotic drug wad encapsulated with the developed ZnO NPs functionalized HA nanocarrier were determined by using FTIR spectroscopy. The structure of the formed ZnO-HA and drug-loaded ZnO-HA was confirmed by FTIR spectroscopy. The FTIR spectrum of (A) HA, (B) hybrid nanocarrier, and (C) CIPRO-encapsulated hybrid nanocarrier were determined (Fig. 1). From Fig. 1A, the peaks are noted in the range of 2917 $cm^{-1}$and 2838 cm^{-1}owing to aliphatic C—H stretching vibrations of the HA [27]. High-intensity broad peaks appeared at 1572 $cm^{-1}$and 1379 $cm^{-1}$for the C═O stretching of

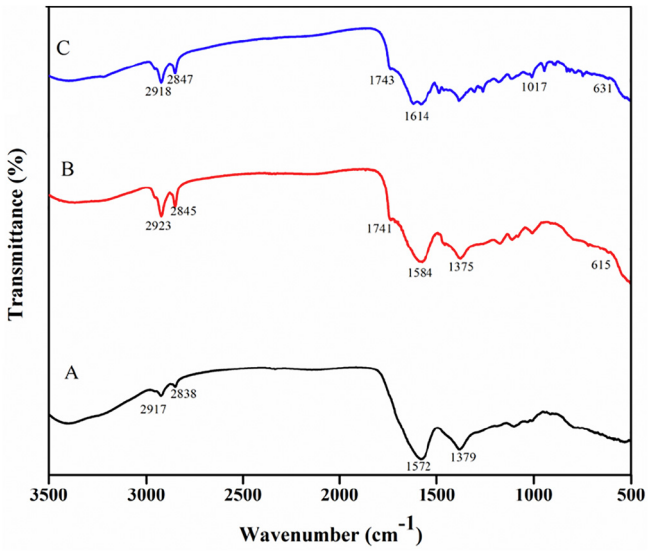

Fig. 1. FTIR spectra of (A) HA; (B) hybrid nanocarrier; and (C) CIPRO-encapsulated hybrid nanocarrier.

the carboxylate groups (COO^-) in HA. The FTIR spectrum of hybrid nanocarrier in Fig. 1B was confirmed by the presence of protonated carboxylic groups (—COO) inducing the ZnO-functionalized HA molecule and asymmetric/symmetric stretching vibrations of C═O, observed at 1741 cm^{-1} [28]. The formation of ZnO was confirmed by the bands occurring in the range of 615–900 cm^{-1}. Encapsulation of CIPRO by the nanocarrier is depicted in Fig. 1C. The signals at 1614 cm^{-1} showed the symmetric and asymmetric stretching vibration of the carboxylate group of CIP anions. The minor shift in 1017 cm^{-1} could be due to the interaction of CIPRO molecules with hybrid nanocarrier.

3.2. X-ray diffraction analysis

The crystalline nature of HA, as synthesized hybrid nanocarrier and drug-encapsulated hybrid nanocarrier was investigated by X-ray diffraction (XRD). The patterns are exhibited in Fig. 2. Pure HA had a single peak at a 2Θ value of 28. This indicates the semi-crystalline nature of HA, and it was functionalized with ZnO forming complete crystalline

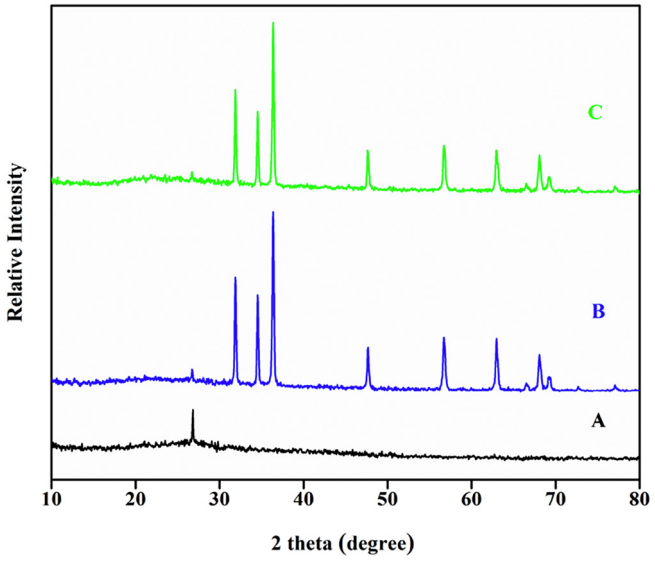

Fig. 2. X-ray diffraction pattern of (A) HA; (B) hybrid nanocarrier; and (C) CIPRO-encapsulated hybrid nanocarrier.

structures. The XRD pattern of HA-ZnO showed intensity peaks at 26.7°, 31.8°, 34.5°, 36.3°, 47.6°, 56.7°, 62.9°, 66.4°, 68.0°, 69.2°, 72.7°, and 77.0°, and it was well correlated with JEPDS file no-79-0205. After encapsulation, the XRD pattern of ZnO-HA-CIPRO retained the intensity of ZnO. This confirmed the presence of Zinc in both carriers and drug-loaded carrier [29]. The crystal size was calculated from the XRD patterns. The average crystal size was 45.53×10^{-9} nm (nanometer) for HA, 39.48×10^{-9} nm for hybrid nanocarrier, and 39.72×10^{-9} nm for drug-encapsulated hybrid nanocarrier.

3.3. Scanning electron microscopy (SEM) analysis

The morphology of ZnO NPs, hybrid nanocarrier, and CIPRO-encapsulated hybrid nanocarrier were investigated using SEM spectroscopy. SEM evaluation provided information on the morphology of (A) ZnO NPs, (B) hybrid nanocarrier, and (C) CIPRO-encapsulated hybrid nanocarrier, illustrated in Fig. 3. Fig. 3A exhibits the well-aggregated plate-like structure of ZnO NPs. Fig. 3B shows the spherical shape of hybrid nanocarrier with diameters in the range of 1 μm, and CIPRO-encapsulated hybrid nanocarrier with diameters in the range of 0.5 μm are shown in Fig. 3C. Moreover, the particles were unevenly distributed owing to low dispersibility, which resulted in the strict conglutination of particles, reducing the probability of forming the spherical particles. This confirmed that the CIPRO-encapsulated hybrid nanocarrier act as an excellent drug-carrying vehicles [30].

3.4. Transmission electron microscopy (TEM) analysis

The shape and size of the hybrid nanocarrier and CIPRO-encapsulated hybrid nanocarrier were revealed by TEM analysis (Fig. 4). The TEM images in Fig. 4A confirm the as-synthesized nanocarriers are in spherical shape. The particles were agglomerated owing to the presence of the hydroxyl groups of HA and cross-linking. Fig. 4B illustrates the CIPRO-encapsulated hybrid nanocarrier; the TEM image clearly shows that the drug molecules were loaded on the carrier, marked with red arrows. This implies that hybrid nanocarrier have larger space for the encapsulation of drugs [31]. The selected area electron diffraction (SAED) pattern exposed the inside of the TEM image, and the SAED spectrum was well correlated with the XRD pattern.

3.5. CIPRO encapsulation efficiency

The potential ability of the synthesized hybrid nanocarrier was determined based on their encapsulation efficiency. The UV spectrum of the CIPRO encapsulation is shown in Fig. 5. This illustrates that CIPRO was loaded onto the nanocarrier through the emulsion method. The encapsulation efficiency increased with increasing time because of the gradual loading on the pores of the hybrid nanocarrier. Consequently, the drug encapsulation efficiency was observed to be nearly 99% at 0 min.

3.6. In-vitro CIPRO release

The drug-releasing properties of the developed carrier were investigated by the commonly used dialysis bag membrane method [32].Various physiological environments, such as pH of the body, significantly influence drug release mechanisms. The pH is the most important factor that triggers sustained drug release from the carriers into target cells. The release behavior of CIPRO from the hybrid nanoparticles was investigated in PBS with media of different pHs: 2.5, 5.5, 6.8, and 8.0. The concentration of the drug and stability of the carriers, as *in-vitro* drug release behavior, was studied using UV–vis spectrophotometry. The λ_{max} values were 334 nm, 316 nm, 297 nm, and 295 nm for pH 2.5, 5.5, 6.8, and 8.0, respectively (Fig. 6). Each pH had its own λ_{max} value, given that aqueous solubility is pH-contingent. Based on pH assessments, CIPRO was slowly released from hybrid nanoparticles for as long as 24 h in all tested media. As the pH increased from acidic to alkaline, the percentage of drug release also increased. The drug release percentages at 24 h were 87.5%, 98.03%, 97.44%, and 97.24% for the pH values of 2.5, 5.5, 6.8, and 8.0, respectively. At pH 5.5, the drug release rate was the highest, because of enhanced solubility, electrostatic interactions, π–π interactions, and hydrogen bonds. Thus, increasing the affinity between the as-synthesized hybrid nanocarrier and CIPRO results in sustained release of the drug [33]. The drug-releasing profile indicated that CIPRO-loaded nanocarrier is pH sensitive. This is because the negatively charged HA was adsorbed onto the positively charged ZnO NPs, owing to the reduced electrostatic repulsion between the ZnO and HA. Addition of HA on to the ZnO could afford further adsorption sites for CIPRO and increase CIPRO adsorption onto the hybrid sites [34].

3.7. In-vitro antibacterial activity of hybrid nanocarrier

3.7.1. MIC and MBC determination

To determine the antibacterial activity of (A) CIPRO, (B) hybrid nanocarrier, and (C) CIPRO-encapsulated hybrid nanocarrier, the broth dilution assay was performed. The attained outcomes showed that the drug at 55 μg ml^{-1} and drug-loaded complex at 25 μg ml^{-1} possess actual antibacterial activity against *B. cereus*. For *P. aeruginosa*, the MIC was found to be 35 μg ml^{-1} for the drug and 15 μg ml^{-1} for the drug-loaded carrier. ZnO NPs are much more effective agents in controlling the growth of various microorganisms, and they are known to kill various bacteria, including MRSA [35]. Carrier alone was kept as a vehicle control and did not possess its own discrete antibacterial efficacy but significantly aided the drug in its antimicrobial potential. Padmavathy et al. [36] reported the bacteriostatic and bactericidal effect of ZnO NPs

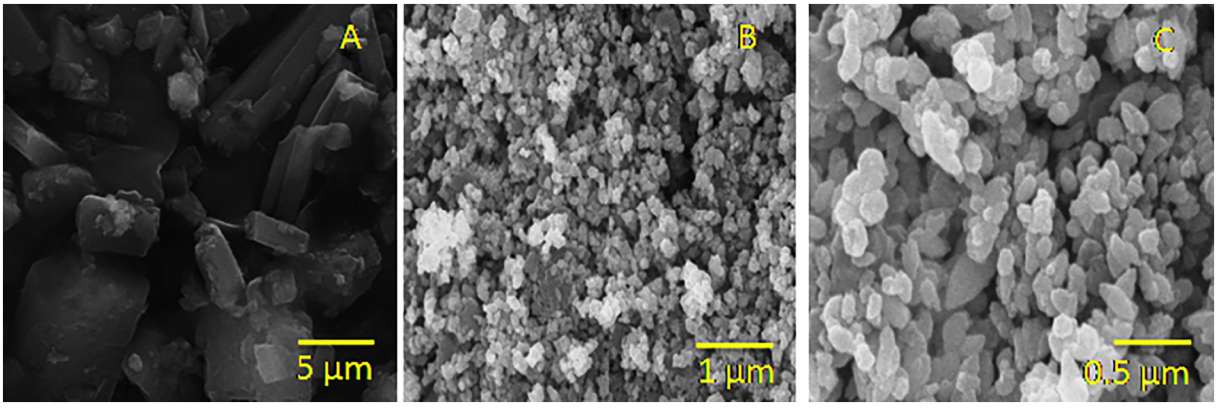

Fig. 3. SEM image of (A) ZnO NPs; (B) hybrid nanocarrier; and (C) CIPRO-encapsulated hybrid nanocarrier.

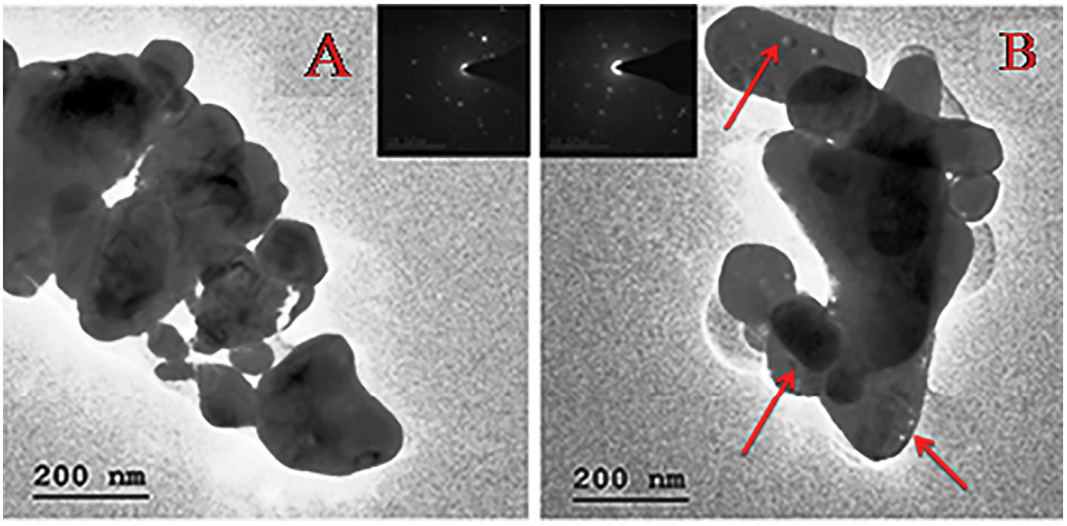

Fig. 4. TEM/SAED image of (A) hybrid nanocarrier; and (B) CIPRO encapsulated hybrid nanocarrier.

at a concentration above 400 μg ml^{-1} against *E. coli*. Lesser MIC relates to higher antibacterial effectiveness. The MBC was determined as 80 μg ml^{-1} and 65 μg ml^{-1} for drug alone and 60 μg ml^{-1} and 30 μg $ml^{-1}$for the drug-loaded carrier against *B. cereus* and *P. aeruginosa*, respectively.

3.7.2. Time-kill kinetics against P. aeruginosa and B. cereus

The time-kill kinetic profiles of the drug and drug-loaded carriers, shown in Fig. 7, revealed variable degrees of bactericidal and bacteriostatic activities on the tested bacterial strains at the tested concentrations. All the concentrations tested had similar killing rates against *B. cereus* and *P. aeruginosa* after 30 min of incubation. The killing rate of drug alone was slower than that of the drug-loaded carrier against *B. cereus* and *P. aeruginosa*; bactericidal activities were only detected after 1 h of incubation at 2× MIC. Treatment with a concentration higher than the MIC of both the drug and drug-loaded complex greatly inhibited the growth of *P. aeruginosa* and *B. cereus* as anticipated. A noteworthy killing efficacy was observed with the drug-loaded carrier even at low exposure time, when compared with that of the drug alone. Complete cell death was observed within 2–3 h of incubation with the drug-loaded carrier and 4–5 h with the drug alone. The augmented sensitivity of *S. aureus* to ZnO NPs has also been reported [37,38]. Accordingly, Sawai [39] has stated the strong affinity between ZnO NPs and *S. aureus* as the cause of the higher activity of the former against this microorganism.

3.7.3. Crystal violet biofilm assay and HCS-live biofilm staining with Hoechst

A wide range of studies regarding the effects of ZnO NPs on bactericidal activity focused on planktonic free-floating bacterial cells suspended in nutrient medium [40,41]. Bacterial biofilms grow and mature on several medical devices, including orthopedic implants, and play a major role in chronic obstinate infection. Given that bacteria entrenched in the biofilm are protected by a self-secreted polymeric matrix, they are often less responsive to traditional antibiotic treatment. Hence, the present study evaluated the inhibition of biofilms by ZnO NPs and determined whether the presence of dissolved HA modifies this tolerance. The drug and drug-loaded carrier were applied as initial attachment inhibitors on the MTP wells, with post inoculation. A visible growth reduction was observed at 1× MIC of drug and drug-loaded

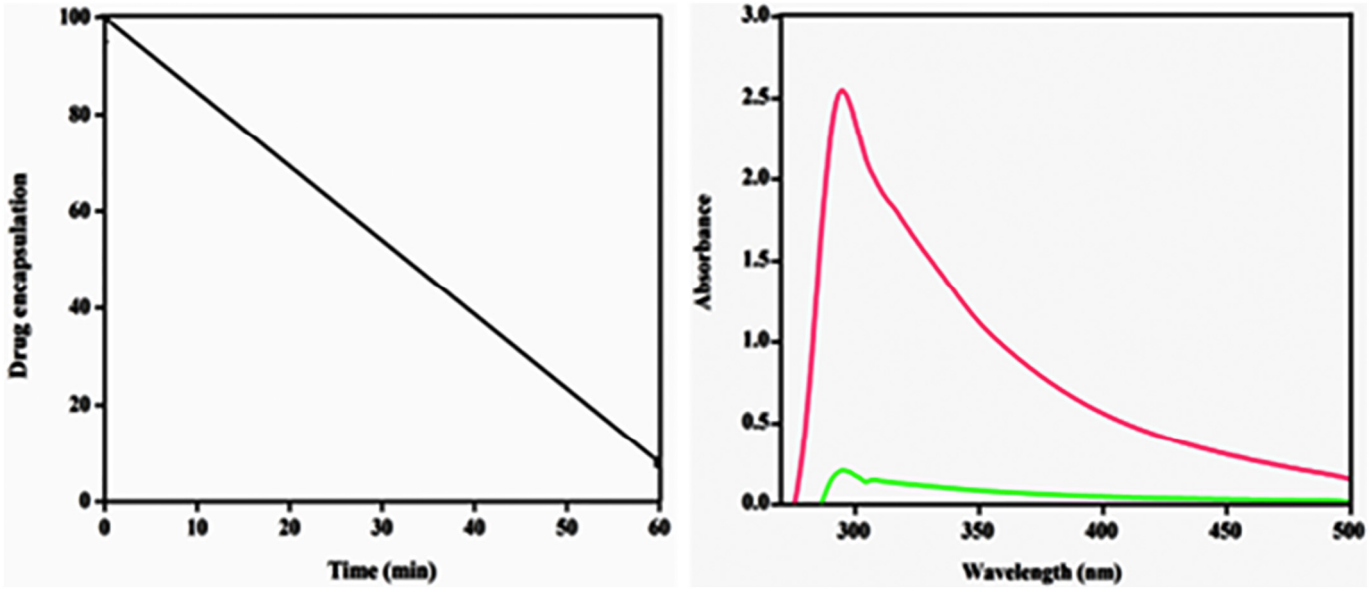

Fig. 5. *In-vitro* drug encapsulation profiles of hybrid nanocarrier.

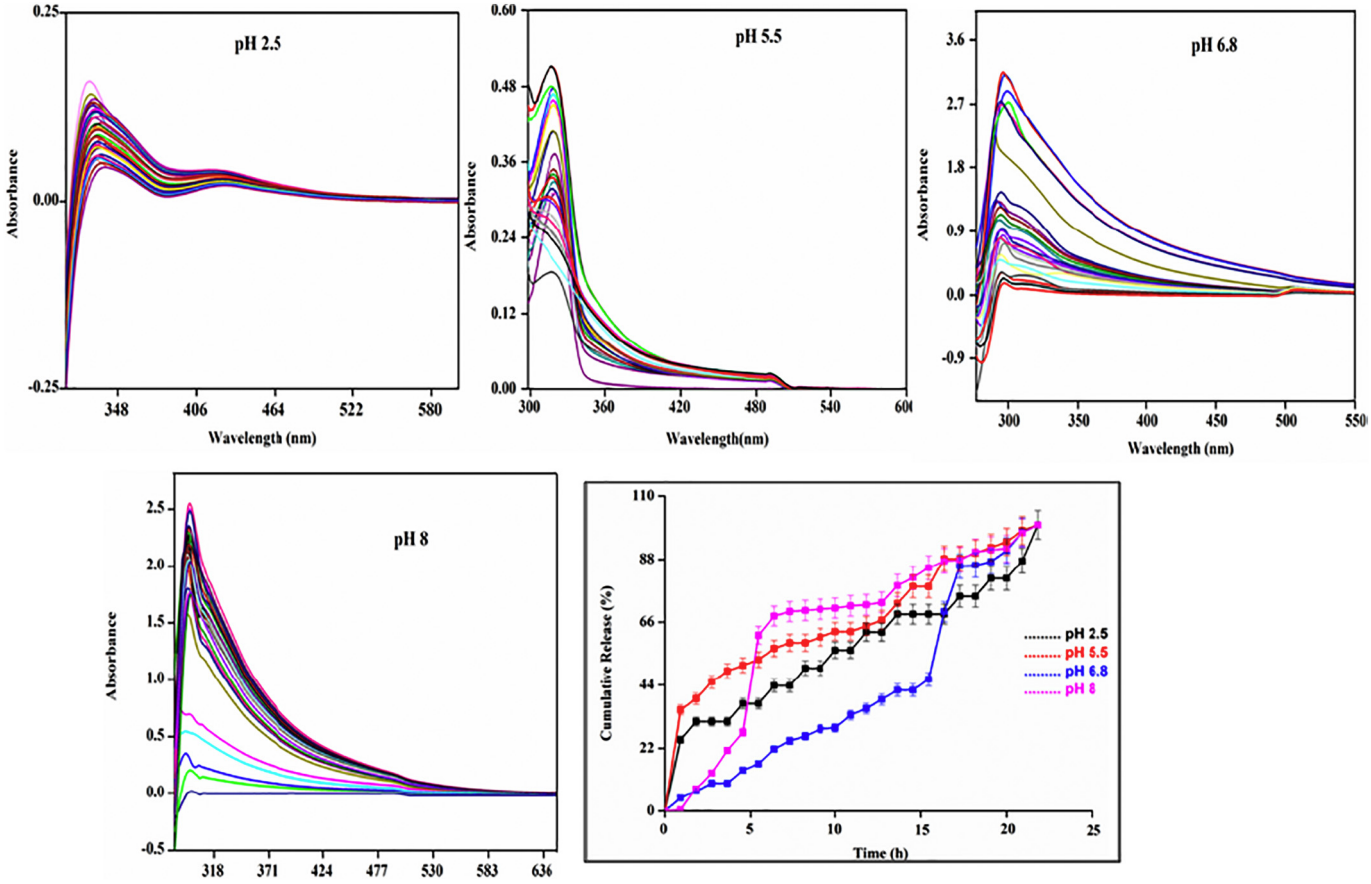

Fig. 6. *In-vitro* drug release profiles of CIPRO-encapsulated hybrid nanocarrier.

carrier. To minimize antimicrobial effects, sub-MIC levels of the drug and drug-loaded carrier were used. At 1/2 MIC, the biofilm formation was decreased by up to 40% and 60% for *B. cereus* and *P. aeruginosa*, respectively, upon treatment with the drug; and by 75% and 85%, respectively, upon treatment with the drug-loaded carrier. Furthermore, phase-contrast micrographs clearly exposed the architecturally complex and dynamic multi-layered matrix construction of *B. cereus* and *P. aeruginosa* biofilms in the control, whereas the drug and drug-loaded carrier (1/2 MIC)–treated micrographs lacked such matrix structures. The observations of the disruption of biofilm formation were supported by high content screening analysis, using Hoechst staining, which showed unstructured biofilm formation upon incubation with the drug (Fig. 8). Reduction in blue fluorescence was recorded in the case of drug treatment.

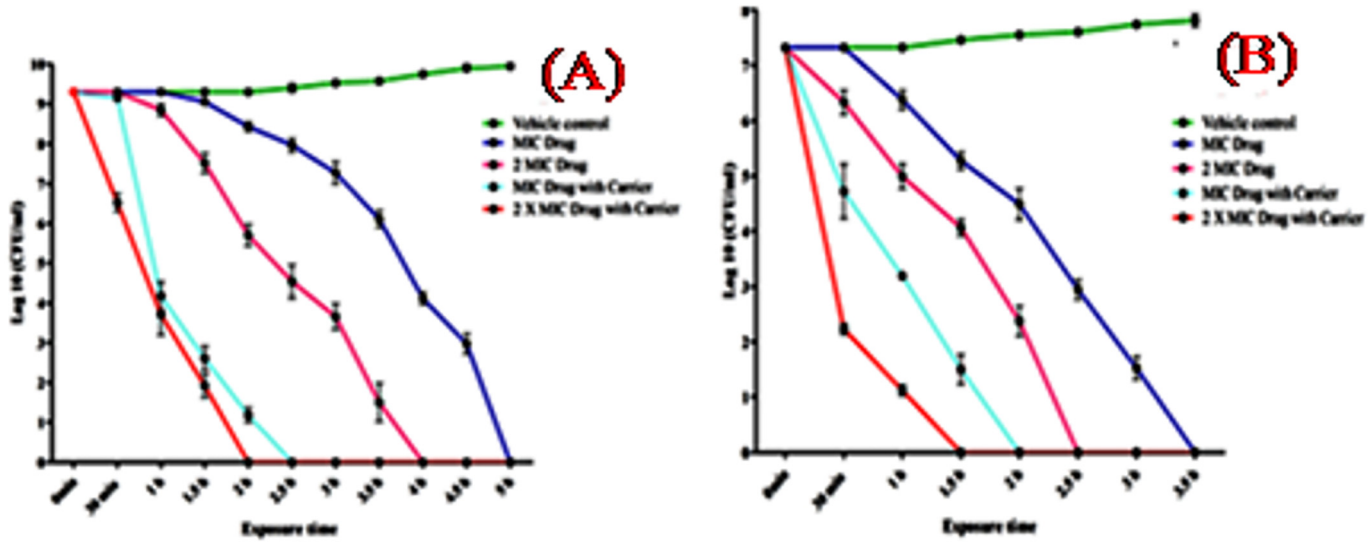

Fig. 7. Time-kill kinetics curve of (A) *Bacillus cereus*; and (B) *Pseudomonas aeruginosa*.

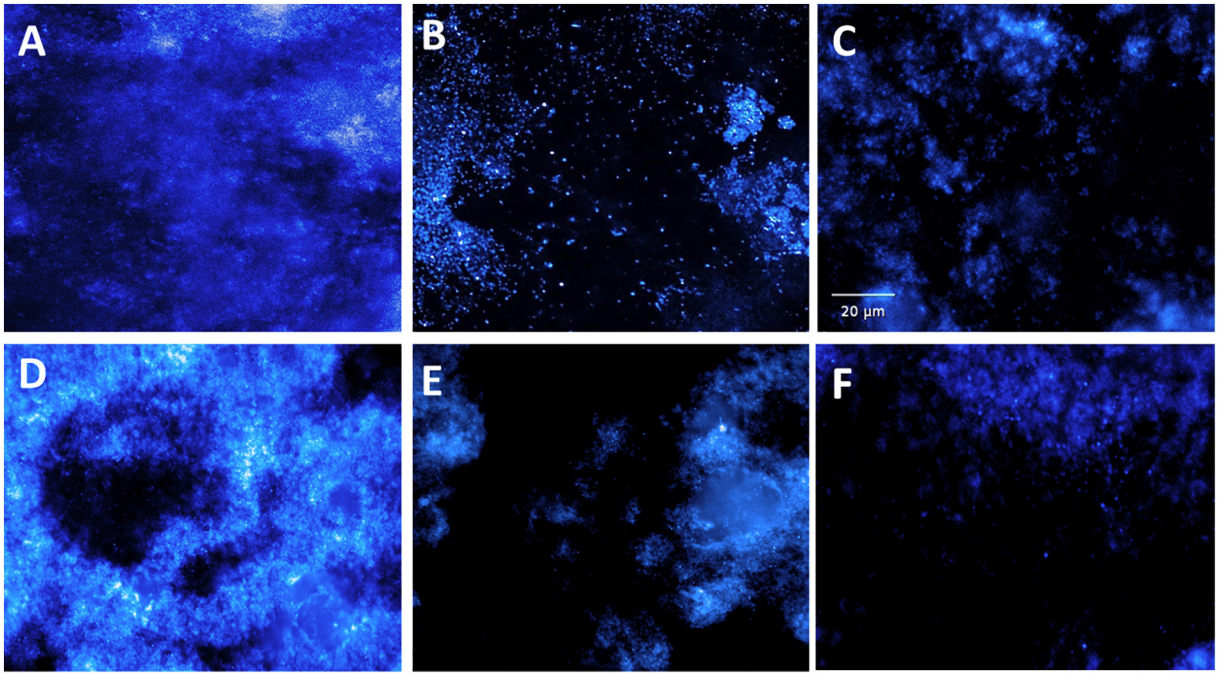

Fig. 8. HCS analysis of biofilm inhibition by Hoechst staining. (A) Control *Pseudomonas aeruginosa* biofilm; (B) *Pseudomonas aeruginosa* biofilm incubated with 1/2 MIC of drug alone; and (C) drug-loaded carrier; (D) control *Bacillus cereus* biofilm; (E) *Bacillus cereus* biofilm incubated with 1/2 MIC of drug alone; and (F) drug-loaded carrier.

3.7.4. Motility and colony-spreading assay

A combination of motility and colony development facilitates bacteria to sense and chase nutrients and reach and up hold their preferred niches for colonization. Therefore, motility appears to play a role principally in the prompt stages of infection, facilitated by colonization and adherence through flagella [42]. The drug and drug-loaded carrier triggered a significant anti-motility effect against both *B. cereus* and *P. aeruginosa*, effectively slowing their growth at the center of the soft

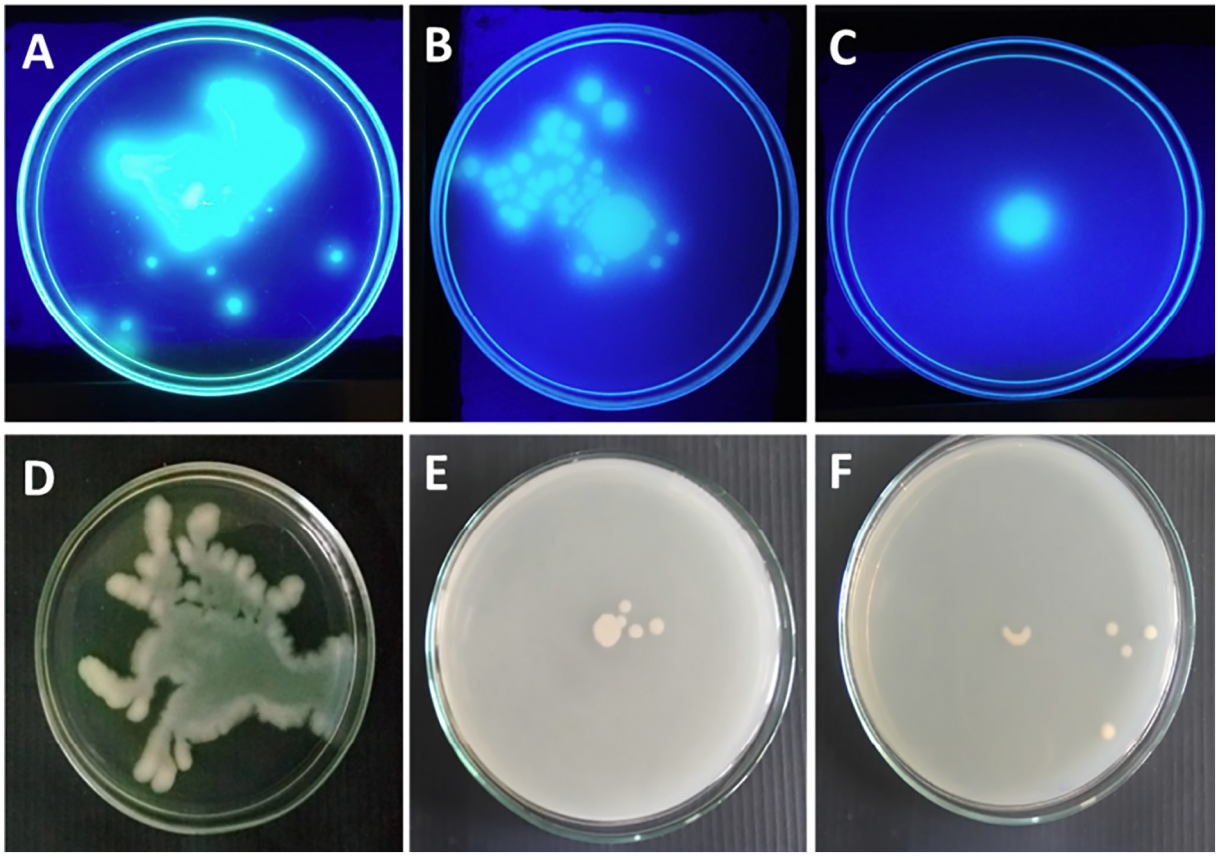

Fig. 9. Motility inhibition. (A) Control *Pseudomonas aeruginosa* spot inoculated; (B) *Pseudomonas aeruginosa* incubated with 1/2 MIC of drug alone; and (C) drug-loaded carrier; (D) control *Bacillus cereus*; (E) *Bacillus cereus* incubated with 1/2 MIC of drug alone; and (F) drug-loaded carrier.

agar plates (Fig. 9). The anti-motility effect limits the range of the bacterial movement in plates, with a limited number of cells, and consequently reduces biofilm formation. For *P. aeruginosa*, pyocyanin synthesis was also inhibited owing to motility arrest.

4. Conclusion

The synthesis of hybrid nanocarrier containing encapsulated CIPRO drugs was demonstrated using simple emulsion techniques. CIPRO was successfully encapsulated in hybrid nanocarrier with high loading absorbance of 295 nm (λ_{max} value). CIPRO can be used as a pH-sensitive drug delivery vehicle, where the drug is released slowly under physiological conditions for as long as 24 h in media at various pHs (2.5, 5.5, 6.8, and 8.0). Nevertheless, at pH 5.5 the drug release rate was the highest. XRD confirmed the crystalline nature of the synthesized hybrid nanocarrier and CIPRO-encapsulated hybrid nanocarrier. SEM and TEM images illustrated the encapsulation of CIPRO into the hybrid nanocarrier, in the range of 200 nm. CIPRO-encapsulated hybrid nanocarrier exhibited higher antibacterial activity against both gram-positive and gram-negative bacteria than did hybrid nanocarrier and drug alone. These results justify the use of this newly developed hybrid nanocarrier as an alternative and suitable carrier for the remedy of bacterial infections, owing to its high biocompatibility, biodegradability, safety, and cost-effectiveness.

Acknowledgements

M. Rajan is grateful to the DST-SERB, Government of India, for financial support under the scheme of "EMEQ" (F. No. - SB/EMEQ-241-2014), New Delhi. M. Rajan thanks the DST-FIST program for the purchase of an FTIR, SEM, and the UGC, for funds under UPE programs for the purchase of a TEM. The authors would like to extend their sincere appreciation to the Deanship of Scientific Research at King Saud University for its funding this Research group No (RG-1436-025).

References

[1] R. Jijie, A. Barras, F. Teodorescu, R. Boukherroub, S. Szunerits, Advancements on the molecular design of nanoantibiotics: current level of development and future challenges, Mol. Syst. Des. Eng. 2 (2017) 349–369.
[2] M. Schmidt, S. Harmuth, E.R. Barth, E. Wurm, R. Fobbe, A. Sickmann, C. Krumm, J.C. Tiller, Conjugation of ciprofloxacin with poly(2 oxazoline)s and polyethylene glycol via end groups, Bioconjug. Chem. 26 (2015) 1950−1962.
[3] M.H. Xiong, Y. Bao, X.Z. Yang, Y.H. Zhu, J. Wang, Delivery of antibiotics with polymeric particles, Adv. Drug Deliv. Rev. 78 (2014) 63–76.
[4] N. Abed, P. Couvreur, Nanocarriers for antibiotics: a promising solution to treat intracellular bacterial infections, Int. J. Antimicrob. Agents 43 (2014) 485–496.
[5] A. Gulzar, S. Gai, P. Yang, C. Li, M.B. Ansari, J. Lin, Stimuli responsive drug delivery application of polymer and silica in biomedicine, J. Mater. Chem. B 3 (2015) 8599–8622.
[6] S. Kariminiaa, A. Shamsipurb, M. Shamsipura, Analytical characteristics and application of novel chitosan coated magnetic nanoparticles as an efficient drug delivery system forciprofloxacin. Enhanced drug release kinetics by low-frequency ultrasounds, J. Pharm. Biomed. Anal. 129 (2016) 450–457.
[7] Wen-Yu Qian, Dong-Mei Sun, Rong-Rong Zhu, Du Xi-Ling, Hui Liu, Shi-Long Wang, pH-sensitive strontium carbonate nanoparticles as new anticancer vehicles for controlled etoposide release, J. Nanomed. 7 (2012) 5781–5792.
[8] M. Karimi, P. Avci, R. Mobasseri, M.R. Hamblin, H. Naderi-Manesh, The novel albumin–chitosan core–shell nanoparticles for gene delivery: preparation, optimization and cell uptake investigation, J. Nanopart. Res. 15 (2013) 1–24.
[9] M.W. Tibbitt, J.E. Dahlman, R. Langer, Emerging frontiers in drug delivery, J. Am. Chem. Soc. 138 (2016) 704−717.
[10] A. Santos, M.S. Aw, M. Bariana, T. Kumeria, Y. Wang, D. Losic, Drug-releasing implants: current progress, challenges and perspectives, J. Mater. Chem. B 2 (2014) 6157–6182.
[11] M.A. Mirza, N. Ahmada, S.P. Agarwal, D. Mahmoodb, M.K. Anwer, Z. Iqbal, Comparative evaluation of humic substances in oral drug delivery, Results Pharma Sci. 1 (2011) 16–26.
[12] M.A. Mirza, S.P. Agarwal, M.A. Rahman, A. Rauf, N. Ahmad, A. Alam, Z. Iqbal, Role of humic acid on oral drug delivery of an antiepileptic drug, Drug Dev. Ind. Pharm. 37 (3) (2011) 310–319.
[13] X. Zhang, R. Bai, Adsorption behavior of humic acid onto polypyrrole-coated nylon 6,6 granules, J. Mater. Chem. 12 (2002) 2733–2739.
[14] G.Z. Kyzas, D.N. Bikiaris, D.A. Lambropoulou, Effect of humic acid on pharmaceuticals adsorption using sulfonic acid grafted chitosan, J. Mol. Liq. 230 (2017) 1–5.
[15] H.-L. Huang, H.-H. Huang, Y.J. Wei, Reduction of toxic Cr(VI)-humic acid in an ionic liquid, Spectrochim. Acta B 133 (2017) 9–13.
[16] P. Patra, S. Mitra, N. Debnath, P. Pramanik, A. Goswami, Ciprofloxacin conjugated zinc oxide nanoparticle: a camouflage towards multidrug resistant bacteria, Bull. Mater. Sci. 37 (2014) 199–206.
[17] W. Castro, M. Navarro, C. Biot, Medicinal potential of ciprofloxacin and its derivatives, Future Med. Chem. 5 (2013) 81—96.
[18] E.C. dos Santos, Z. Rozynek, E.L. Hansen, R. Hartmann-Petersen, R.N. Klitgaard, A. Løbner-Olesen, L. Michels, A. Mikkelsen, T.S. Plivelic, H.N. Bordallo, J.O. Fossum, Ciprofloxacin intercalated in fluorohectorite clay: identical pure drug activity and toxicity with higher adsorption and controlled release rate, RSC Adv. 7 (2017) 26537–26545.
[19] N. Ehlert, M. Badar, A. Christel, S.J. Lohmeier, T. Luessenhop, M. Stieve, T. Lenarz, P.P. Muellerb, P. Behrens, Mesoporous silica coatings for controlled release of the antibiotic ciprofloxacin from implants, J. Mater. Chem. 21 (2011) 752–760.
[20] K.P. Miller, L. Wang, B.C. Benicewiczb, A.W. Decho, Inorganic nanoparticles engineered to attack bacteria, Chem. Soc. Rev. 44 (2015) 7787–7807.
[21] K. Lingaraju, H.R. Naika, K. Manjunath, R.B. Basavaraj, H. Nagabhushana, G. Nagaraju, D. Suresh, Biogenic synthesis of zinc oxide nanoparticles using *Ruta graveolens* (L.) and their antibacterial and antioxidant activities, Appl. Nanosci. 6 (2016) 703–710.
[22] D. Raoufi, Synthesis and microstructural properties of ZnO nanoparticles prepared by precipitation method, Renew. Energy 50 (2013) 932–937.
[23] R. Pati, R.K. Mehta, S. Mohanty, A. Padhi, M. Sengupta, B. Vaseeharan, C. Goswami, A. Sonawane, Topical application of zinc oxide nanoparticles reduces bacterial skin infection in mice and exhibits antibacterial activity by inducing oxidative stress response and cell membrane disintegration in macrophages, Nanomedicine 10 (2014) 1195–1208.
[24] H.R. Ghorbani, F.P. Mehr, H. Pazoki, B.M. Rahmani, Synthesis of ZnO nanoparticles by precipitation method, Orient. J. Chem. 31 (2015) 1219–1221.
[25] K. Rani, Recent applications of hybrid nanobiomaterial as non-viral gene delivery vehicles, Int. J. Pharm. Res. 8 (2016) 10–15.
[26] K. Suganya, A. Krithika, K. Govindan, D. Asha, M. Murugan, Monitoring surfactant mediated defence of gastrointestinal Proteus mirabilis DMTMMK1 against pathogenic consortia of *Vibrio cholera*, RSC Adv. 7 (2017) 20969–20980.
[27] F. Sakellariadou, Spectroscopic studies of humic acids from subsurface sediment samples collected across the Aegean Sea, Mediterr. Mar. Sci. 7 (2006) 11–17.
[28] P. Boguta, Z. Sokołowska, Interactions of Zn(II) ions with humic acids isolated from various type of soils. Effect of pH, Zn concentrations and humic acids chemical properties, PLoS One 11 (4) (2016) 1–20.
[29] H. Nabipour, M.H. Sadr, G.R. Bardajee, Synthesis and characterization of nanoscale zeolitic imidazolate frameworks with ciprofloxacin and their applications as antimicrobial agents, New J. Chem. 41 (2017) 7364–7370.
[30] G.S. Kumar, R. Govindan, E.K. Girija, In situ synthesis, characterization and in vitro studies of ciprofloxacin loaded hydroxyapatite nanoparticles for the treatment of osteomyelitis, J. Mater. Chem. B 2 (2014) 5052.
[31] W. Wu, W. Yao, X. Wang, C. Xie, J. Zhang, X. Jiang, Bioreducible heparin-based nanogel drug delivery system, Biomaterials 39 (2015) 260–268.
[32] M. Rajan, V. Raj, Formation and characterization ofchitosan-polylacticacid-polyethylene glycol-gelatin nanoparticles: a novel biosystem for controlled drug delivery, Carbohydr. Polym. 98 (2013) 951–958.
[33] M.H. Mashhadizadeh, M. Amoli-Diva, Drug-carrying amino silane coated magnetic nanoparticles as potential vehicles for delivery of antibiotics, J. Nanomed. Nanotechol. 3 (2012) 4.
[34] W. Wang, J. Cheng, J. Jin, Q. Zhou, Y. Ma, Q. Zhao, A. Li, Effect of humic acid on ciprofloxacin removal by magnetic multifunctional resins, Sci. Rep. 6 (2016), 30331.
[35] N. Jones, B. Ray, K.T. Ranjit, A.C. Manna, Antibacterial activity of ZnO nanoparticle suspensions on a broad spectrum of microorganisms, FEMS Microbiol. Lett. 279 (2007) 71–76.
[36] N. Padmavathy, R. Vijayaraghavan, Enhanced bioactivity of ZnO nanoparticles-an antimicrobial study, Sci. Technol. Adv. Mater. 9 (2008), 035004.
[37] L.K. Adams, D.Y. Lyon, P.J. Alvarez, Comparative eco-toxicity of nanoscaleTiO_2, SiO_2, and ZnO water suspensions, Water Res. 40 (2006) 3527–3532.
[38] G. Applerot, N. Perkas, G. Amirian, O. Girshevitz, A. Gedanken, Coating of glass with ZnO via ultrasonic irradiation and a study of its antibacterial properties, Appl. Surf. Sci. 256 (2009) S3–S8.
[39] J. Sawai, Quantitative evaluation of antibacterial activities of metallic oxide powders (ZnO, MgO and CaO) by conductimetric assay, J. Microbiol. Methods 54 (2003) 177–182.
[40] V. Aruoja, H.C. Dubourguier, K. Kasemets, A. Kahru, Toxicity of nanoparticles of CuO, ZnO and TiO_2 to microalgae Pseudokirchneriellasubcapitata, Sci. Total Environ. 407 (2009) 1461–1468.
[41] K.R. Raghupathi, R.T. Koodali, A.C. Manna, Size-dependent bacterial growth inhibition and mechanism of antibacterial activity of zinc oxide nanoparticles, Langmuir 27 (2011) 4020–4028.
[42] C. Josenhans, S. Suerbaum, The role of motility as a virulence factor in bacteria, Int. J. Med. Microbiol. 291 (2002) 605–614.